



**AALBORG UNIVERSITY**  
DENMARK

**Aalborg Universitet**

## **Artificial Intelligence-Based Control Design for Reliable Virtual Synchronous Generators**

Xu, Qianwen; Dragicevic, Tomislav; Xie, Lihua Xie; Blaabjerg, Frede

*Published in:*  
I E E E Transactions on Power Electronics

*DOI (link to publication from Publisher):*  
[10.1109/TPEL.2021.3050197](https://doi.org/10.1109/TPEL.2021.3050197)

*Publication date:*  
2021

*Document Version*  
Accepted author manuscript, peer reviewed version

[Link to publication from Aalborg University](#)

*Citation for published version (APA):*  
Xu, Q., Dragicevic, T., Xie, L. X., & Blaabjerg, F. (2021). Artificial Intelligence-Based Control Design for Reliable Virtual Synchronous Generators. *I E E E Transactions on Power Electronics*, 36(8), 9453 - 9464. [9318554]. <https://doi.org/10.1109/TPEL.2021.3050197>

### **General rights**

Copyright and moral rights for the publications made accessible in the public portal are retained by the authors and/or other copyright owners and it is a condition of accessing publications that users recognise and abide by the legal requirements associated with these rights.

- Users may download and print one copy of any publication from the public portal for the purpose of private study or research.
- You may not further distribute the material or use it for any profit-making activity or commercial gain
- You may freely distribute the URL identifying the publication in the public portal -

### **Take down policy**

If you believe that this document breaches copyright please contact us at [vbn@aub.aau.dk](mailto:vbn@aub.aau.dk) providing details, and we will remove access to the work immediately and investigate your claim.

# Artificial Intelligence based Control Design for Reliable Virtual Synchronous Generators

Qianwen Xu, *Member, IEEE*, Tomislav Dragicevic, *Senior Member, IEEE*, Lihua Xie, *Fellow, IEEE*  
and Frede Blaabjerg, *Fellow, IEEE*

**Abstract**—Virtual synchronous generator (VSG) is a promising solution for inertia support of the future electricity grid to deal with the frequency stability issues caused by the high penetration of renewable generations. However, the power variation in power electronic interface converters caused by VSG emulation increases the stress on power semiconductor devices and hence has a negative impact on their reliability. Unlike existing works that only consider stability for VSG control design, this paper proposes a double-artificial neural network (ANN) based method for designing VSG inertia parameter considering simultaneously the reliability and stability. First, a representative frequency profile is generated to extract various VSG power injection profiles under different inertia values through detailed simulations. Next, a functional relationship between inertia parameter ( $H$ ) and lifetime consumption (LC) of VSG is established by the proposed double-ANN reliability model:  $ANN_t$  provides fast and accurate modeling of thermal stress in the semiconductor devices from a given operating profile; With the aid of  $ANN_t$ ,  $ANN_{LC}$  is built for fast and accurate estimation of LC for different inertia parameters in the next step. The proposed approach not only provides a guideline for parameter design given a certain LC requirement, but can also be used for optimal design of VSG parameter considering reliability and other factors (e.g. inertia support in this paper). The proposed technique is applied to a grid-connected VSG system as a demonstration example.

**Index Terms**—Virtual synchronous generators, virtual inertia, stability, reliability, artificial intelligence.

## I. INTRODUCTION

THE utilization of renewable energy resources (e.g. PV, wind turbines) as distributed generation (DG) units have attracted great attention all over the world for the environmental friendly requirements [1]. Power electronics converters are widely used as the interfaces for the integration of the DG units into the grid [2]. In the past, grid frequency is regulated by synchronous generators (SGs), which can provide inertia by absorbing or delivering the kinetic energy stored in their rotors and turbines [3]. However, with the high penetration of DG interface converters in the grid, which have very small or no inertia and damping properties, power system inertia is reduced and the frequency stability is becoming a considerable concern [4].

To increase grid inertia and provide frequency support in the future power electronics based power system, the virtual

synchronous generator (VSG) technology has been proposed by mimicking the essential characteristics of the SGs so that the rotating inertia can be emulated in power electronics interface converters [4], [5]. There are various implementations of VSGs in literature, like virtual synchronous machine [6], virtual synchronous generator (VSG) [7]–[9], synchronverter [10], synchronous power controller [11], etc. The inertia characteristics emulated by VSGs can contribute to the total inertia of the grid and enhance the transient frequency stability. A prominent feature of VSG is that its parameters (e.g., the virtual inertia constant  $H$  and damping factor  $D$ ) are not constrained by the physical factors as the real SGs; on the contrary, they are control parameters that can be manually designed to have expected dynamic performance. There are several works discussing the parameter design of the VSG. In [8], [11], the closed-loop characteristic equation of the VSG power loop is derived and a relationship between dynamic performance and design parameters (inertia constant and damping coefficient) is developed. In [12], the coupling effect between active power loop and reactive power loop is analyzed and the inertia coefficient is designed based on the small signal model from the perspective of system stability. Ref. [13] discusses the parameter constraints considering stability. In [14], the influences of parameters on the dynamic response of VSGs are investigated, including peak time, settling time and overshoot. However, none of the existing works consider the impact of design parameters on reliability of the VSG, which is a critical concern in power electronics based power systems.

Power electronic converters are reported to be the most unreliable parts in renewable energy systems [15], e.g., wind power systems [16], photovoltaic (PV) power systems [17] and fuel cell power systems [18]. In particular, power semiconductor devices are the most vulnerable links in power electronic converters [15]. Power processing will pose stress on these sensitive devices, affect their lifetimes and finally impact system reliability. Previously, reliability assessment is achieved in a statistic way assuming constant failure rates regardless of their mission profiles and MIL-HDBK-217 handbook has been widely adopted to predict lifetime of power electronic devices [19], [20]. Recent trend in reliability of power electronics systems is moving towards physics-of-failure based reliability assessment by identifying root-causes of failures [16][18], [21]–[26]. Refs [21] and [22] present experimental validation of linear cumulative damage theory in the lifetime prediction of power semiconductor devices. In [23], a comprehensive review of failure and lifetime prediction of power devices is presented, which summarizes different techniques typically

Q. Xu is with Electric Power and Energy Systems Division, KTH Royal Institute of Technology, Sweden (e-mail: qianwenx@kth.se)

T. Dragicevic is with the Department of Electrical Engineering, Technical University of Denmark, Denmark. (email: tomdr@elektro.dtu.dk)

L. Xie is with School of Electrical and Electronic Engineering, Nanyang Technological University, Singapore (e-mail: elhxie@ntu.edu.sg)

F. Blaabjerg is with the Department of Energy Technology, Aalborg University, Denmark (e-mail: fbl@et.aau.dk)

used for measuring the junction temperature for lifetime prediction. Ref. [16] proposes a mission profile based system level reliability analysis of DC/DC converters for a fuel cell power application. Ref. [24] proposes a reliability oriented design of modular multilevel converters for medium-voltage static synchronous compensator. In [25], a thermal stress based design of smart transformer is proposed. Reliability oriented design tools are development for PV converters in [17], [26]. In [18], selection of power converters in DFIG wind turbine is presented with enhanced system-level reliability. For all the state-of-art reliability works [15][17], [20]-[25], failures of power semiconductor devices are mainly induced by thermal stress and are assessed by mean junction temperature and junction temperature cycles over the operating period. The power loading and ambient temperature profiles are normally considered as mission profiles of power semiconductor devices, as they have direct contribution to the thermal stress. Lifetime consumption (LC) of a power semiconductor device is estimated using the obtained junction temperature profile from thermal stress under a specific mission profile, which requires detailed simulations or experiments. To assist long-term simulation, a look-up table method is conventionally applied to transform the mission profile into thermal cycles for LC estimation [17], [26]. However, as the lookup table method is based on linear interpolation, it cannot learn the nonlinear relationship between the input and output data; moreover, it is not suitable for high dimensional data mapping, which is inevitable when impact of both system design parameters and mission profile on the system's lifetime needs to be studied. A promising solution to overcome the drawbacks is to use an artificial neural network (ANN), which has the capability to approximate nearly any functions of input/output data with arbitrary precision [27], [28]. Inspired by wide applications of ANN in prediction [28], [29], it is possible to use ANN to map LC of power semiconductor device from various mission profiles to achieve faster and more accurate LC estimation.

The VSG technology is important for inertia support in the future power electronics based power systems. By controlling the DG interface inverters as VSGs to enhance grid inertia and provide frequency support, the loading profiles of VSGs will be different from the original loading profiles. This will affect LC of power semiconductor devices in the DG interface inverters, which are commonly designed based on the original loading conditions (i.e. power outputs of DGs) without considering inertia support. Current methods for parameter design of VSGs only consider system dynamics and stability, while their impacts on power electronics reliability are not taken into consideration. As power semiconductor devices are normally the weakest links in the power electronic converter systems, the LC of power semiconductor device is selected as the system reliability metric. In this paper, we propose a double-artificial neural network (ANN) based approach for designing a more reliable grid connected VSG system with the consideration of both inertia (stability) and LC (reliability). First, a representative frequency profile is extracted to generate different power injection profiles under different control parameters (i.e., inertial constant  $H$ ). Then a double-ANN model is built to map  $H$  to LC:  $ANN_t$  is

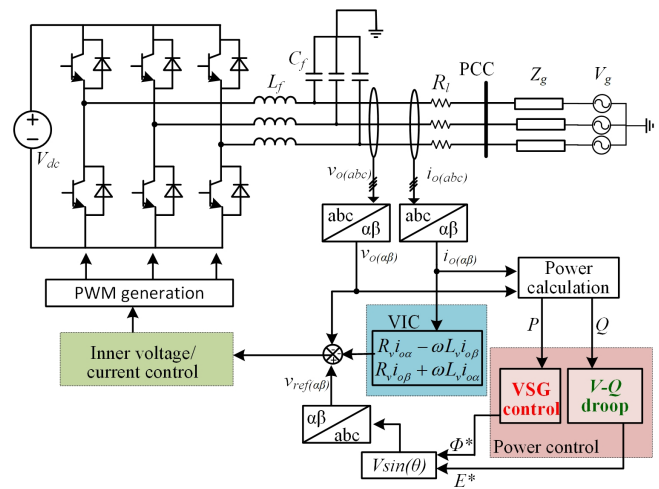


Fig. 1. A grid-connected VSG system.

constructed and trained to translate mission profiles (power injection profile and ambient temperature profile) into the thermal loading profile based on detailed simulation data; Based on  $ANN_t$  and the generated power injection profile under different values of  $H$ , LC of power semiconductor device in DG inverter is calculated, and these data are used to train  $ANN_{LC}$ , which models the relationship between input data ( $H$ ) and output data (LC).  $ANN_{LC}$  provides a quick estimation of LC given different inertia parameters. Then the overall system optimization function for parameter design is formulated with the combined objectives of inertia and LC. The main contributions of this paper are summarized as follows:

- 1) Unlike conventional VSG design methodologies only considering inertia, it optimizes the control parameter considering both inertia performance and LC.
- 2) A double ANN model is proposed to provide a quantitative relationship for how the designed inertia parameter will impact reliability.
- 3) A novel profile reduction method is developed to map a long-term mission profile to a representative short-term mission profile with the same stochastic features.
- 4) A guideline is developed about how to optimize the control parameter considering LC and other performance factors (e.g. the inertia requirement and the transient stability requirement) simultaneously.

This paper is organized as follows: Section II describes VSG system model and the impact of inertia parameter. The double-ANN based technique is proposed for VSG parameter design by simultaneously considering stability and reliability in Section III. The proposed technique is demonstrated and verified in Section IV by a case study. Conclusions are drawn in Section V.

## II. SYSTEM DESCRIPTION AND INERTIA DESIGN

There are several different implementations of the VSG. In this paper, a relatively common topology is adopted, as shown in Fig. 1 [5], [31]. An energy storage unit is applied with the VSG control technique to mimic the swing equation of

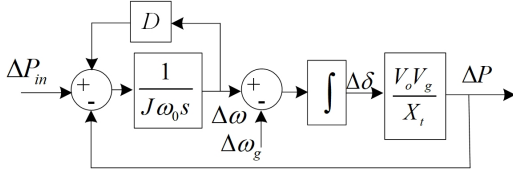


Fig. 2. The small signal model of the grid connected VSG system.

the SGs in order to support the grid frequency fluctuation and provide inertia. A typical three phase voltage source inverter is connected to the grid at the point of common coupling through an LC filter  $L_f$  and  $C_f$ . Grid impedance is denoted as  $Z_g$ . The inverter operates in the voltage source mode with the inner voltage and current regulation using PR controllers in synchronous reference frame. The virtual impedance control (VIC) is implemented to emulate an impedance connected in series with the grid line impedance between the inverter output and the PCC to make the equivalent line impedance inductive [30]. The VSG control is implemented in the power control loop to provide virtual inertia, damping and droop control. As only one VSG is studied here, droop control is not included in VSG control block.

In various implementations of VSG control, the mimicking of rotor inertia is similar but the forms of damping vary, e.g.,  $D(\omega - \omega_0)$  and  $D(\omega - \omega_g)$  [5], [31], where  $D$  is the damping factor,  $\omega_0$  is the nominal angular frequency,  $\omega_g$  is the grid angular frequency. Note that the former one combines droop and damping, while the latter considers separate droop and damping terms. Here,  $D(\omega - \omega_g)$  is adopted as an application example, as its damping factor will not impact droop coefficient and thus it can be designed to get desired system dynamics. The swing equation is expressed as

$$P_{in} - P - D(\omega - \omega_g) = J\omega \frac{d(\omega - \omega_g)}{dt} \quad (1)$$

where  $P_{in}$  is the set-point value of active power,  $P$  is the measured output power of VSG,  $\omega$  is the angular frequency of the virtual rotor,  $J$  represents the moment of inertia of the virtual rotor; as the deviation of  $\omega$  is relatively small,  $J\omega$  can be approximated by  $J\omega_0$  [8].

The small signal model of the VSG system in Fig. 1 is shown in Fig. 2 [8]. Then the transfer function from power reference to the output power is derived as

$$\Delta P = \Delta P_{in} \frac{\frac{V_o V_g}{X_t J \omega_0}}{s^2 + \left(\frac{D}{J \omega_0}\right)s + \frac{V_o V_g}{X_t J \omega_0}} \quad (2)$$

where  $X_t$  is the equivalent inductive line impedance considering the virtual impedance.

The transfer function is equivalent to a standard second order differential equation [8]:

$$\Delta P = \Delta P_{in} \frac{\omega_n^2}{s^2 + 2\xi\omega_n s + \omega_n^2} \quad (3)$$

with the natural frequency  $\omega_n$  and damping ratio  $\xi$  expressed as  $\omega_n = \sqrt{\frac{V_t V_g}{X_t J \omega_0}}$  and  $\xi = \frac{D}{2\sqrt{V_t V_g J \omega_0}}$ .

Based on (3),  $J$  and  $D$  can be tuned to have the desired dynamic response. Given a specific inertia  $J$  and the required damping ratio  $\xi$ ,  $D$  can be designed as

$$D = 2\xi \sqrt{\frac{V_t V_g J \omega_0}{X_t}} \quad (4)$$

The variables in (1) are transformed into per-unit values so that the system dynamic response is not constrained by the power ratings of power converters, i.e., frequency response of a 1 MVA system will be the same as that of a 1-kVA system as long as their parameters are equivalent in per-unit forms [32]:

$$P_{in\_pu} - P_{pu} - D_p(\omega_{pu} - \omega_{g\_pu}) = 2H \frac{d(\omega_{pu} - \omega_{g\_pu})}{dt} \quad (5)$$

where  $H = \frac{J\omega_0^2}{2S_N}$ ,  $D_p = \frac{D\omega_0}{S_N}$ ,  $S_N$  is the power rating of the DG.

Once the inertia constant  $H$  is determined, the corresponding  $J$  and  $D$  can be derived according to (5) and (4) to have expected system dynamics. Therefore, we assume that  $H$  is the only control parameter to be designed.

Fig. 3 shows the dynamic response of a VSG to support the grid frequency variation with different inertia values. At 3s, the grid frequency ramps down from 50 Hz to 49.8 Hz with the rate at 2 Hz/s. The VSG is to provide inertia support of the grid. As can be observed, a larger  $H$  will provide a larger inertia support, and thus a larger  $H$  is expected from inertia's perspective. However, a larger  $H$  also means more energy extracted from the energy source for inertia support, as shown in the response of power  $P$  in the first plot of Fig. 3. The plot reveals that the VSG has different power outputs with different values of  $H$  for different levels of inertia support, which will definitely impact the lifetime consumption (LC) of power devices in the VSG and finally impact the reliability of the VSG. Therefore, it is clear that  $H$  is a key parameter that affects both inertia and reliability.

In existing works, there are no general rules for designing  $H$ . Some works select  $H$  based on parameters from the conventional SGs (0-10s) [4], or from stability [10]-[13]. But none of them consider reliability. Therefore, an ANN based methodology is proposed to provide a quantitative relationship of inertia parameter and reliability, and develop a guideline for the optimal design of  $H$  considering both stability and reliability.

### III. PROPOSED DOUBLE-ANN DESIGN APPROACH

Fig. 4 shows the proposed double-ANN framework for designing a grid connected VSG system, which involves representative mission profile generation, double-ANN based LC modeling and design optimization considering both reliability and inertia.

#### A. Representative mission profile generation

The LC of power semiconductor device is significantly influenced by the system operating conditions, e.g., the loading profile and ambient temperature profile. Unlike the original renewable energy sources, which normally operate at maximum

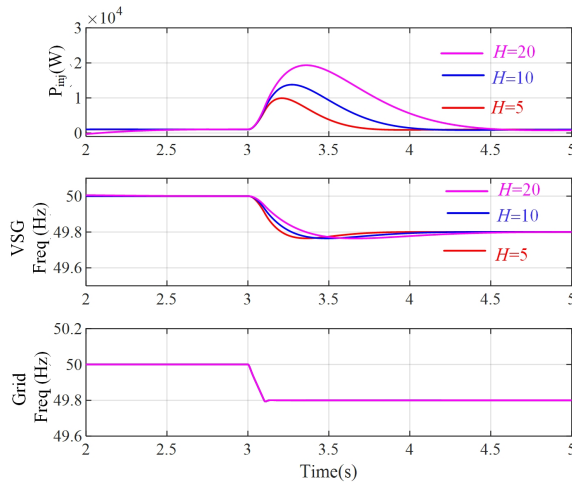


Fig. 3. Dynamic response of a VSG to support the grid frequency variation with different  $H$ .

power point tracking mode or power control mode, a VSG will provide extra power injection to support system inertia during the grid frequency fluctuations. This extra injected power passes through the grid connected inverter, increases power loss and thermal stress, and as a result, causes increased LC. Thus the power injection profile  $P_{inj}$  of VSG consists of the original power set-point value  $P_{in}$  and the extra power injection caused by virtual inertia support. With different values of  $H$ , different loading profiles  $P_{inj}$  will be generated and consequently, the LC will be affected.

A problem encountered in this step is to get the power injection profile from a detailed simulation over a long period with the grid frequency profile. This is because of the long simulation time required for simulating a detailed simulation model over a long operating period, e.g., for a one-minute operating period, the simulation running time is almost 1 minute.

To avoid running lengthy numerical simulations, the long-term frequency profile can be represented by a short-term frequency profile that has similar statistical properties. Based on Kolmogorov-Smirnov (k-s) test result for the long-term frequency profile, the data follows the standard normal distribution. For the normal distribution, the statistical properties are determined by the mean value and standard deviation [33]. To be representative, the short-term frequency profile is generated to have the same normal distribution properties as the long-term frequency profile. Then the short-term frequency profile is applied to the system in Fig. 1 with various values of  $H$  to generate the power injection profile of VSG.

### B. Double-ANN Lifetime Consumption Model

After the power injection profiles of VSG for different  $H$  constants are obtained, they are applied to the ANN-based power semiconductor converter thermal model in order to estimate the LC of the power devices.

The main failure mechanism of power device is related to the thermal cycling, which is translated from the mission profiles and can lead to wear-out failures, e.g. bond wire lift

off. In a standard design for reliability approach, the lifetime evaluation involves translation of the mission profile to thermal loading profile, interpretation of thermal loading profile and LC modeling. To assist the simulation for the LC with a long-term mission profile (e.g., an annual mission profile), a lookup table model is normally constructed to translate the mission profile to thermal loading profile. However, as the electrothermal model is nonlinear, to enhance the accuracy of lookup table method, numerous simulations are required to have more breakpoints in the lookup tables; and the whole process for estimating LC of power electronic converters usually consists of several lookup tables (e.g., one lookup table for device model, one lookup table for power loss model and one lookup table for thermal model in [26]). Thus the process to build an accurate lookup table based model is quite complicated, requiring the knowledge of inner physical models [26]. And when a large amount of data is processed, lookup table based method is still time-consuming.

As a widely used machine learning algorithm, ANN offers a promising solution for dealing with nonlinear relationships with a large amount of data [28]. In the following parts, a double ANN based approach is used for fast and accurate mapping of the relationship from control parameter  $H$  to LC.

1)  $ANN_t$ : First,  $ANN_t$  is constructed to translate the mission profiles (power injection profile and ambient profile) into the thermal loading profile.

An ANN is based on a collection of artificial neurons, which models the neurons in a biological brain. The neurons receive input, change their internal state (activation) according to that input, and produce output depending on the input and activation. A general multi-layer feedforward ANN consists of an input layer, one or more hidden layers and an output layer, where each layer has several neurons. The basic knowledge of an ANN is illustrated in Appendix. For  $ANN_t$ , it has 2 neurons in the input layer (for two input variables: power injection  $P_{inj}$  and ambient temperature  $T_a$ ) and 2 neurons in the output layer (for two output variables: mean junction temperature  $T_{jm}$  and cycle amplitude  $\Delta T_j$ ). The hidden layers can be determined by trial and error from training and test data. Fig. 5 shows an example of  $ANN_t$ .

The training and test data of  $ANN_t$  are obtained by simulating the detailed models of power converter with the associated thermal model. The mission profiles of power injection and ambient temperature are taken as the input variables of the  $ANN_t$  and the resulted junction temperature variation profile is the output.

2)  $ANN_{LC}$ : Next,  $ANN_{LC}$  is built to estimate the LC according to different values of  $H$ .

Similar as  $ANN_t$ ,  $ANN_{LC}$  is a multi-layer feedforward ANN. It has one neuron at input layer (for virtual parameter  $H$ ) and one neuron at output layer (for LC), as shown in Fig. 6.

The training and test data of  $ANN_{LC}$  are datasets of  $H$  and the corresponding LC. Given different values of  $H$ , the corresponding LC is estimated based on the following procedure:

As described in Section III.A, power injection profiles  $P_{inj}$  are obtained by simulating VSG system in Fig. 1 with various



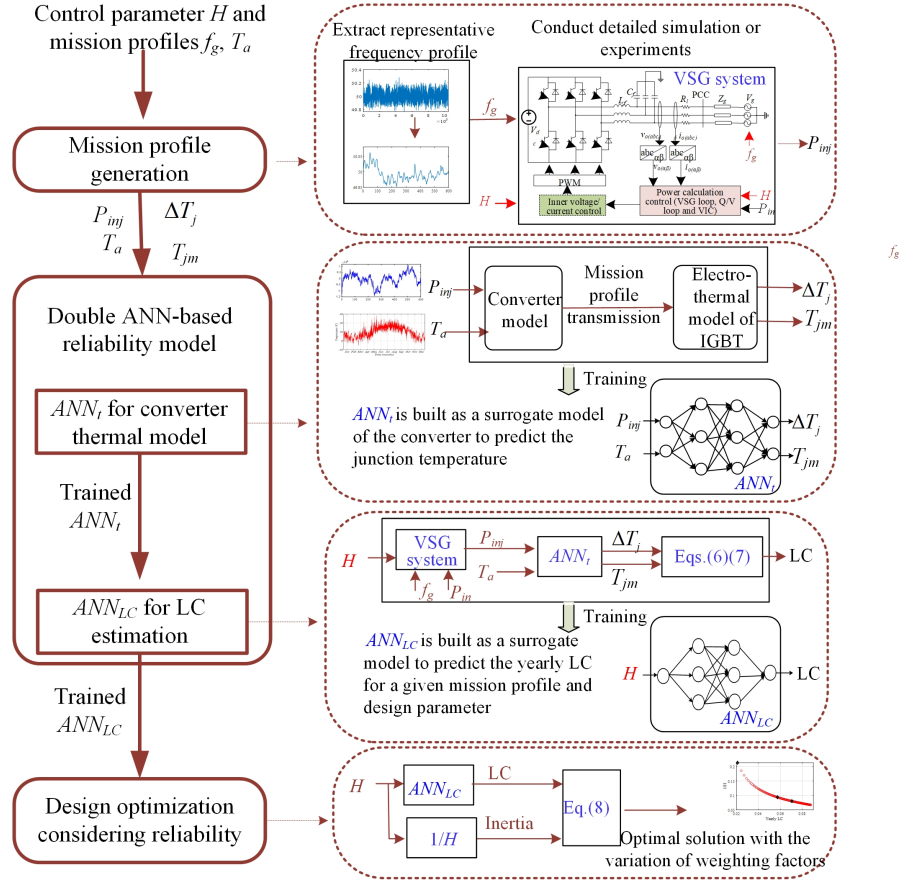


Fig. 4. The proposed double-ANN framework.

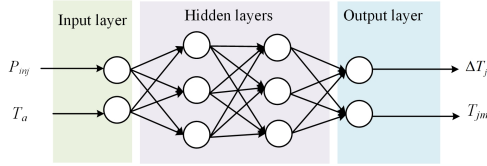


Fig. 5. Structure of  $ANN_t$ .

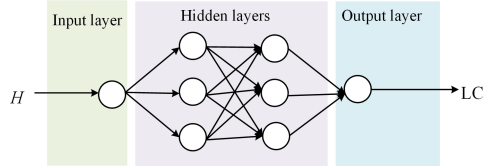


Fig. 6. Structure of  $ANN_{LC}$ .

selections of  $H$  under the representative short-term frequency profile. Then the power injection profile  $P_{inj}$  and ambient temperature profile  $T_a$  are fed to  $ANN_t$  to generate the junction temperature profile  $T_j$ .

The junction temperature profile provides information of the mean junction temperature  $T_{jm}$ , cycle amplitude  $\Delta T_j$  and cycle period  $t_{on}$ . As the junction temperature profile usually contains mission profile dynamics, which is irregular, a cycle counting algorithm such as a rainflow analysis is needed for the thermal cycling interpretation [17], [26]. For example, the rainflow counting algorithm can decompose an

irregular profile into several regular cycles according to the amplitude value  $\Delta T_j$ , average value  $T_{jm}$  and period of the cycle  $t_{on}$ . By applying this method to the junction temperature profile, the number of cycles at a certain cycle amplitude  $\Delta T_j$ , mean junction temperature  $T_{jm}$  and cycle period  $t_{on}$  can be obtained.

With the obtained information, the number of cycles to failure is estimated as [17]:

$$N_f = A \times (\Delta T_j)^\alpha \times (ar)^{\beta_1 \Delta T_j + \beta_0} \times \left[ \frac{C + (t_{on})^\gamma}{C + 1} \right] \times \exp\left(\frac{E_a}{k_b \times T_{jm}}\right) \times f_d \quad (6)$$

where  $N_f$  is the number of cycles to failure.  $T_{jm}$  is the mean junction temperature,  $\Delta T_j$  is the cycle amplitude and  $t_{on}$  is cycle period, which are obtained from the cycle counting method. Other coefficient parameters are given in Table I.

Based on Miner's rule [17], the LC of the power device is obtained as

$$LC = \sum_i \frac{n_i}{N_{fi}} \quad (7)$$

where  $n_i$  is the number of cycles for a certain  $\Delta T_j$ ,  $T_{jm}$  and  $t_{on}$ , which is obtained from the rainflow analysis;  $N_{fi}$  is the number of cycles to failure for the specific stress condition. For instance, if the number of cycles  $n_i$  is counted from a one year mission profile, the corresponding LC will represent a yearly LC of the power device. When the value of LC accumulates to

unity (i.e., 100%), the power electronics device is considered to fail.

By following the procedure described above,  $ANN_{LC}$  can be constructed with the input data ( $H$ ) and corresponding output data (LC).

### C. Optimization model considering both inertia and lifetime consumption

The trained  $ANN_{LC}$  maps the control parameter  $H$  to yearly LC, which provides the basis for optimal parameter design of  $H$  considering both reliability and inertia.

As discussed, the control parameter  $H$  impacts both inertia and LC and we want to optimize  $H$  from the perspective of reliability and inertia simultaneously. One objective is to minimize LC, which can be directly obtained by  $ANN_{LC}$  given different values of  $H$ . From the inertia's perspective, the mechanism for inertia enhancement is essentially increasing  $H$  [4]. Therefore, another optimization objective is selected as the maximization of  $H$ , or equivalently, minimization of  $1/H$ . Thus the overall cost function for optimizing  $H$  with inertia and reliability is formulated as

$$f(H) = LC^2 + w_1 \left( \frac{1}{H} \right)^2 \quad (8)$$

where  $w_1$  is the weighting factor to balance the importance between the two terms, it is a user-defined parameter based on the customer requirement.

By solving  $f(H)$ , the optimal  $H$  can be obtained considering both LC and inertia with different values of weighing factor  $w_1$ .

It should be mentioned that, the cost function in (8) can be revised by taking more factors into consideration. For example, system dynamic performance indices related to inertia, such as RoCoF, frequency nadir and settling time [4], can also be selected as optimization terms.

This method is also flexible for the design of other control parameters considering reliability, like droop control parameter. The study of droop control parameter with LC is briefly discussed in Appendix B.

## IV. CASE STUDY

The proposed methodology in Fig. 4 is applied to a grid-connected VSG system in Fig. 1 as a demonstration example.

TABLE I  
LIFETIME MODEL PARAMETERS OF AN IGBT MODULE

Variables	Value
$A$	$3.4368 * 10^{14}$
$\alpha$	-4.923
$\beta_0$	1.942
$\beta_1$	$-9.012 * 10^{-3}$
$C$	1.434
$\beta_1$	-1.208
$f_d$	0.6204
$a_r$	0.28
$E_a$	0.06606eV
$k_b$	$8.6173324 * 10^{-5} eV/k$

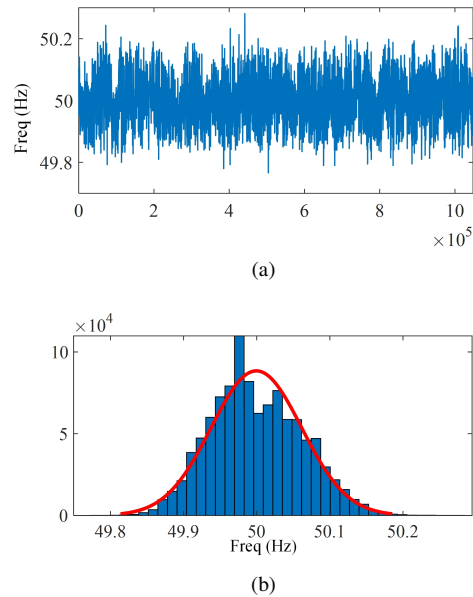


Fig. 7. One-month grid frequency profile in Great Britain with its normal distribution.

The system parameters are listed in Table II. Here the damping ratio  $\xi$  is selected as 0.707 as it offers a good compromise between rise time and settling time [39]. The proposed method is applied in the VSG system in Fig. 1 as an application example, and the detailed procedure described in Section III and Fig. 4 is demonstrated.

### A. Representative mission profile generation

A representative mission profile is generated to shorten the simulation time. Fig. 7a shows one-month grid frequency profile in Great Britain [34] with 1s resolution. Its normal distribution is shown in Fig. 7b. with a mean of 49.9995 Hz and standard deviation at 0.062. To get a representative short-term frequency profile, a 10-minute frequency profile is generated with the same statistical properties as Fig. 7. The generated representative frequency profile is shown in Fig. 8a with its normal distribution in Fig. 8b. Then a yearly frequency profile can be generated using the short-term frequency profile.

The generated frequency profile is fed into the system described in Fig. 1 with the variation of  $H$  to generate the power injection profiles  $P_{inj}$  of VSG system. Fig. 9 shows

TABLE II  
SYSTEM PARAMETERS

Variables	Description	Value
$V_{dc}$	Input voltage	650V
$V_{ac}$	Grid voltage	220V
$f_s$	Switching frequency	5kHz
$\omega_0$	Nominal angular frequency	50Hz
$L_f, C_f$	LC filter	1.8mH, 0.25mF
$L_v, R_v$	Virtual impedance	4mH, 0Ω
$k_{pv}, k_{rv}$	Voltage controller	2, 100
$k_{pc}, k_{rc}$	Current controller	10, 100
$S_N$	Power rating	50kW
$\xi$	Damping ratio	0.707

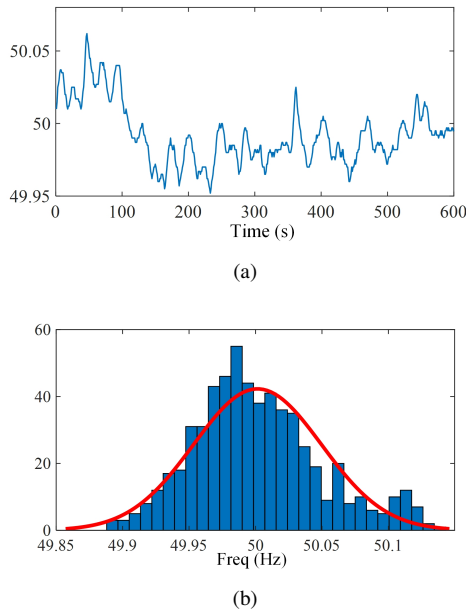


Fig. 8. Generated representative frequency profile with its normal distribution.

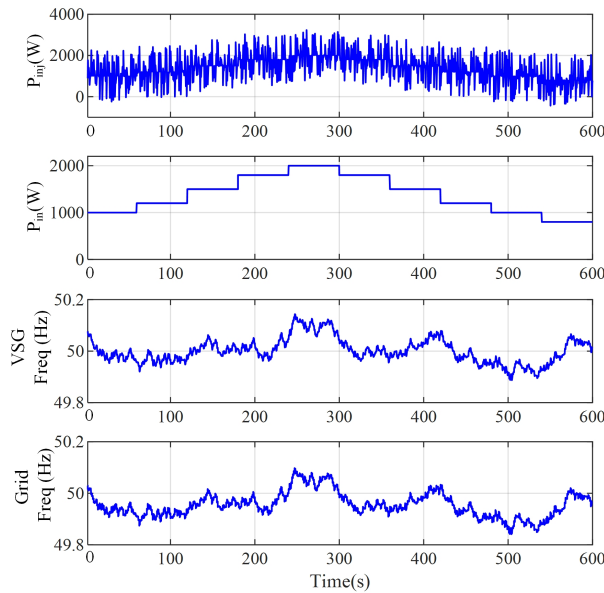


Fig. 9. Simulation results of power injection of VSG  $P_{inj}$ , the original power set-point profile  $P_{in}$ , VSG frequency and grid frequency with  $H$  selected to be 10.

simulation results of total power injection of VSG  $P_{inj}$ , the original power set-point profile  $P_{in}$ , VSG frequency and grid frequency with  $H$  selected to be 10 as an example. Note that  $P_{in}$  is usually given by the operator, here it is given as the second plot in Fig. 9 as an example. As can be observed, with frequency fluctuations, VSG injects or absorbs extra power accordingly to supply inertia.

### B. Double-ANN model training

Double-ANN model is trained based on data from detailed simulations using the feedforward neural network model.

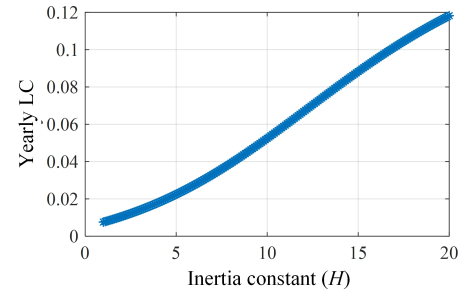


Fig. 10. Yearly LC of the VSG with different values of  $H$  (2:0.1:20).

1)  $ANN_t$ :  $ANN_t$  is constructed according to Section III. B.1. Numerous simulations of the power converter model are conducted with the input data sweeping at  $P_{inj} = 50 : 50 : 1000(W)$  and  $T_a = -10 : 5 : 40$  to generate the corresponding output data of  $T_j$ . There are 231 (i.e.,  $21 \times 11$ ) sets of input/output data. The training data are normalized and fed to a feedforward neural network model in deep learning toolbox in Matlab to get  $ANN_t$ . To determine the structure of  $ANN_t$ , training results are compared for different ANN structures with one or more hidden layers and different numbers of neurons in each layer. In this study, the number of hidden layers is selected to be 3 neurons in both hidden layers, which is the simplest network that provides excellent performance.

2)  $ANN_{LC}$ :  $ANN_{LC}$  is constructed according to Step III.B.2. Given different values  $H$  (2:1:20), corresponding 19 sets of power injection profile  $P_{inj}$  are obtained, as described in Section IV.A. The ambient temperature is another mission profile that impacts LC of power device. Considering that our focus is the impact of power injection profile, ambient temperature is fixed at  $20^\circ C$ . The mission profiles  $P_{inj}$  and  $T_a$  are next fed into  $ANN_t$  to get the thermal cycling profile  $T_j$  immediately. Then the rainflow counting algorithm is applied to get the number of cycles at a certain cycle amplitude, mean junction temperature and cycle period. The yearly LC of the power device in VSG inverter is calculated based on (6) and (7).

The structure of  $ANN_{LC}$  is determined by following the same procedure as  $ANN_t$ . Taking values of  $H$  (2:1:20) as input and corresponding LC values as output data of  $ANN_{LC}$ , doing normalization and feeding them into a feedforward ANN,  $ANN_{LC}$  is trained.

### C. Design optimization considering reliability

The trained  $ANN_{LC}$  can be used for selecting control parameter given a certain LC requirement. Fig. 10 presents the yearly LC of the VSG with different selection of  $H$  (2:0.1:20). It shows that LC increases with the increase of inertia parameter. If reliability requirement of the yearly LC is less than 0.03,  $H$  should be selected less than 6.

The trained  $ANN_{LC}$  can also be applied for design optimization considering LC and inertia using Eq. (8), as illustrated in Section III. C and Fig. 4. To solve the cost function in (8) is equivalent to solve a multi-objective problem. To solve a multi-objective problem, the simplest and most



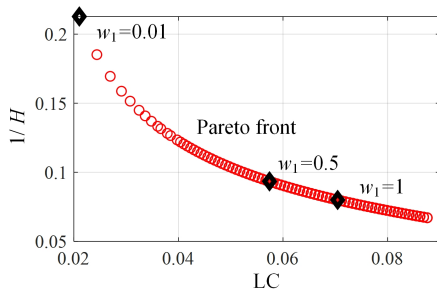


Fig. 11. Optimal yearly LC and reciprocal of inertia ( $1/H$ ) with the sweeping of  $w_1$  at 0.01:0.01:1.2

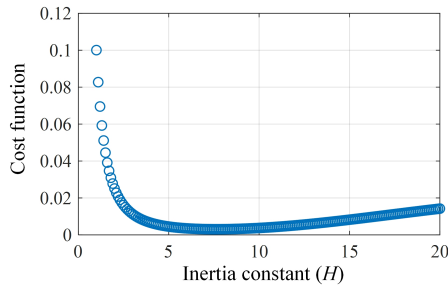
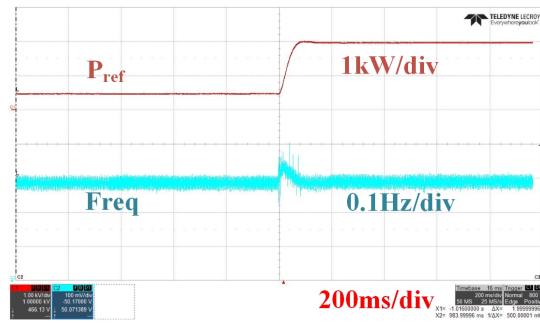


Fig. 12. Cost value with the variation of inertia value  $H$  when weighting factor is selected at 0.1.

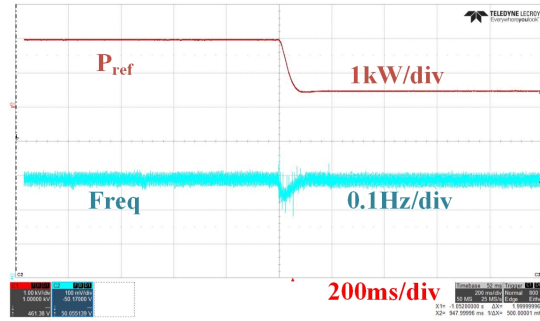
common approach is the weight-sum method, achieved by multiplying each objective function by a weighting factor and summing up all weighted objective functions [35]. The weighting factors are usually scaled to make their summation to be one. The relative value of the weights generally reflects the relative importance of the objectives. The weights can be used in two ways. The designer may either set the weighting factors to reflect preferences before the problem is solved, or systematically alter weights to yield different Pareto optimal points.

Here as the problem is a two-objective problem, for simplicity, we set the weighting factor of  $LC^2$  as 1 and the weighting factor of  $(1/H)^2$  as  $w_1$  in (8), so we only have one weighting factor  $w_1$  to be altered. By alternating  $w_1$  value, we can get the Pareto front of the feasible space of the problem (8), denoted as red line in Fig. 11, which is a set of optimal solutions under different values of  $w_1$  ( $w_1=0.01:0.01:1.2$ ). Three optimal points corresponding to  $w_1=0.01, 0.5$  and  $1$  are highlighted in Fig. 11 as an example to show the balance between LC and inertia with different values of  $w_1$ . With the increasing weight in inertia, a larger optimal inertia value (i.e., smaller  $1/H$ ) is obtained, while this results in an increase of LC. For example, if we want to ensure the LC to be less than 0.06, and to maximize the inertia, we can select inertia as 11 (i.e.,  $1/H=0.09$ ), the corresponding  $w_1$  is around 0.5. Therefore, if inertia support capability is more important, we can select the  $H$  based on Fig. 11 to have optimal inertia support capability with guaranteed requirement of LC.

Fig. 12 shows the cost value with the variation of inertia value  $H$  when weighting factor is selected at 0.1. The optimal solution of  $H$  for this weighting factor can be obtained by finding the lowest value in the plot, which can then be applied



(a)



(b)

Fig. 13. Experimental result for inertia constant  $H$  selected at 10. (a) when the active power reference steps up from 500W to 2kW; (b) when the active power reference steps down from 2kW to 500W.

for parameter design of VSG.

To compare the lookup table method and the proposed method for reliability evaluation, a lookup table based model is built based on [26] consisting of three lookup tables (one lookup table for device model, one lookup table for power loss model and one lookup table for thermal model). The lookup table method and the proposed method are conducted in matlab in a laptop with an Intel i7-8550 CPU and 8 GB of RAM. For the lookup table method, the running time under the 600s power injection profile is 125.670926s. For the proposed method, the running time is 14.249055s, which reduces 89% computational time. Therefore, the lookup table method is more complicated to build and has much higher computational time. While for our method, we only need to know input and output data obtained from simulations, and we can obtain fast and accurate results.

#### D. Experimental verification for inertia support

Hardware in the loop experiments are conducted in RT-lab OP5600 Simulator platform in Energy Research Institute @ NTU to verify the control parameter design for inertia providing capability. The same parameters listed in Table II are adopted. Fig. 13 shows the experimental result for the inertia constant  $H$  selected at 10, when the active power reference steps up from 500W to 2kW and steps down from 2kW to 500W. Fig. 14 shows the result with the same variation for inertia constant  $H$  selected at 2. It shows that, a higher inertia constant  $H$  will have more smooth frequency variation, and the maximum frequency deviation during transient is much

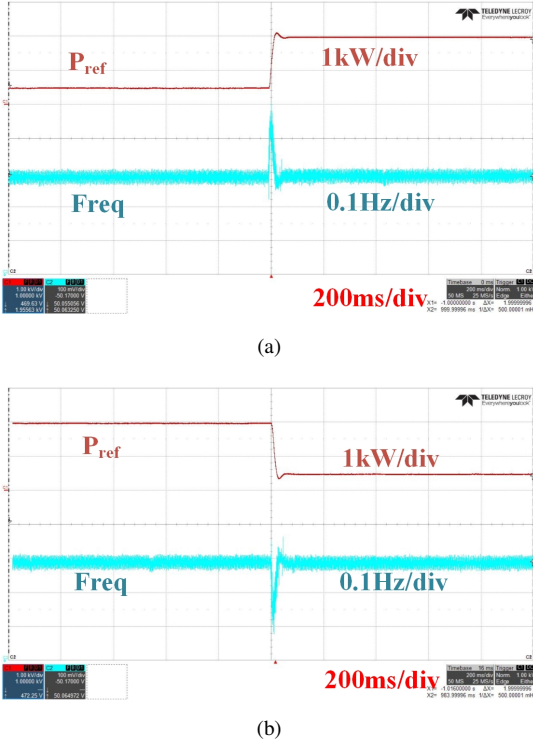


Fig. 14. Experimental result for inertia constant  $H$  selected at 2. (a) when the active power reference steps up from 500W to 2kW; (b) when the active power reference steps down from 2kW to 500W.

smaller, which verifies the design goal of inertia that a higher inertia constant  $H$  will lead to higher inertia support.

## V. CONCLUSION

Unlike existing VSG works that only considers stability, this paper proposes a double-ANN based method for designing VSG inertia parameter ( $H$ ) considering both reliability and stability. First, a representative frequency extraction method is proposed to avoid numerous lengthy simulations for generating power injection profiles under different inertia parameters. Next, a double-ANN reliability model is constructed for fast and accurate estimation of lifetime consumption of power device. Finally, the trained double-ANN model is combined with the other performance factors (such as inertia in this paper as an example) to formulate the cost function for optimal design of inertia parameter. The proposed approach is applied in a grid-connected VSG system as a demonstration example. It provides a guideline about how the inertia constant should be selected within the acceptable damage in device reliability. It could also help the system operators to develop a business model in the future for converter inertia support considering reliability and other performance factors.

## APPENDIX

### A. Basic knowledge of ANN

An artificial neural network (ANN) is based on a collection of artificial neurons, which models the neurons in a biological brain. A typical ANN structure consists of two basic types of components, the neurons for processing information and the

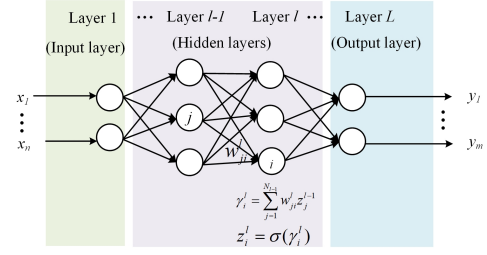


Fig. A1. A general structure of an artificial neural network.

links for interconnections. The feedforward multilayer network structure is a commonly used structure for ANN [27]. Assume there are  $L$  layers. The first layer is called the input layer, which consists of  $n$  neurons ( $n$ =the number of input variables). The last layer is called the output layer, which consists of  $m$  neurons ( $m$ = the number of output variables). The rest layers, i.e. layers 2 to  $(L-1)$ , are hidden layers. Let the number of neurons in the  $l$  th layer be  $N_l$ ,  $l=1,2,\dots,L$ . Define the parameter  $w_{ji}$  to represent the weight of the link between the  $j$ th neuron in the  $(l-1)$ th layer and the  $i$ th neuron in the  $l$ th layer. Fig. A1 presents a general structure of an ANN.

Each neuron processes the information in two steps [28]. First, collect the information from the neurons from the previous layer, given by

$$\gamma_i^l = \sum_{j=1}^{N_{l-1}} w_{ji}^l z_j^{l-1} \quad (\text{A1})$$

where  $\gamma_i^l$  is the weighted sum information for the  $i$ th neuron in the  $l$ th layer, which can be seen as the input for that neuron;  $N_l$  is the number of neurons in the  $l$ th layer,  $l=1,2,\dots,L$ ;  $w_{ji}^l$  is the weight of the link between the  $j$ th neuron in the  $(l-1)$  th layer and the  $i$ th neuron in the  $l$ th layer;  $z_j^{l-1}$  represents the output of  $j$ th neuron in the  $(l-1)$  th layer.

Second, the weighted sum information in (A.1) is processed by an activation function to get the final output of the neuron as  $z_i^l$ , given by

$$z_i^l = \sigma(\gamma_i^l) \quad (\text{A2})$$

The activation function  $\sigma(\cdot)$  can be selected as Sigmoid, Tanh, ReLU, Softmax, etc. Here the widely used sigmoid function is selected, which is given by

$$\sigma(\gamma) = \frac{1}{1 + e^{-\gamma}} \quad (\text{A3})$$

Then the output the neurons in the  $l$ th layer will be fed to the neuros in the next layer for process.

With the input vector  $(x_1, \dots, x_n)^T$ , the process of ANN for prediction can be summarized as [28]:

$$\begin{aligned} z_i^1 &= x_i, i = 1, 2, \dots, N_1 & N_1 &= n \\ z_i^l &= \sigma \left( \sum_{j=1}^{N_{l-1}} w_{ji}^l z_j^{l-1} \right), i = 1, 2, \dots, N_l & & \\ y_i &= z_i^L, i = 1, 2, \dots, N_L & N_L &= m \end{aligned} \quad (\text{A4})$$

where  $(y_1, \dots, y_m)^T$  is the predicted output vector of ANN.

To get a proper ANN model to solve the problem, a suitable number of hidden layers and neurons should be selected

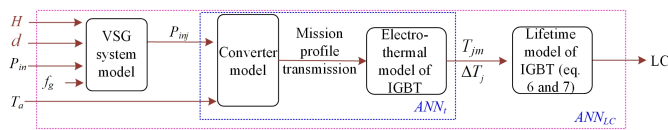


Fig. A2. The procedure of calculating LC of power converters with the variation of droop coefficient  $d$  and inertia constant  $H$ .

first. In general, the choice of hidden layers depends on the characteristic of data. More hidden layers are adopted to characterize more complex relationship, yet more data are also required [36]. How to select the number of hidden neurons remains an open question, and they are selected based on experience or the trial and error process, by trying different neurons during training process to get an acceptable accuracy.

The training process of ANN is to use training data to obtain a proper set of weight parameters  $w_{ji}^l$  to minimize the estimation error of ANN output variables with the real output variables. The properness is evaluated by a loss function, which is usually a mean-square-error function. The backpropagation (BP) training algorithm is widely adopted to get a proper set  $w_{ji}^l$  [37]. The training process of ANN can be achieved by many software packages, like Deep Learning Toolbox in Matlab, Kares, pytorch and tensorflow. In our work, Deep Learning Toolbox in Matlab is used [38]. By feeding the input data and real output data as the training data into the ANN, we can get a well-trained ANN model.

### B. Extension of the proposed method considering droop parameter impact on reliability

This method is flexible to be extended to study the impact of other control parameters (e.g. droop parameter) on reliability. The study of droop parameter is the same as the procedure for  $H$  in Fig. 2. First, we can have different droop parameters to run the simulation and get the power injection profiles  $P_{inj}$ , and then we feed the power injection profiles  $P_{inj}$  to  $ANN_t$  to get the thermal profile and calculate the corresponding LC. Then we can build the relationship between input (i.e., droop coefficient  $d$  and inertia constant  $H$ ) and output (i.e., LC) to train  $ANN_{LC}$ . The procedure is described in Fig. A2. The training process is similar as to be described in Section IV. B. Therefore, the proposed double-ANN method can be extended to study the impact of droop parameters on reliability, and we can also achieve reliability oriented droop parameter design. As the focus of this work is to study the impact of VSG inertia emulation on reliability, the study of droop parameter is not emphasized.

## REFERENCES

- [1] M. H. Bollen, "The smart grid: Adapting the power system to new challenges," *Synthesis Lectures on Power Electronics*, vol. 2, no. 1, pp. 1–180, 2011.
- [2] F. Blaabjerg, R. Teodorescu, M. Liserre, and A. V. Timbus, "Overview of control and grid synchronization for distributed power generation systems," *IEEE Transactions on Industrial Electronics*, vol. 53, no. 5, pp. 1398–1409, 2006.
- [3] P. Kundur, N. J. Balu, and M. G. Lauby, *Power system stability and control*, vol. 7. McGraw-hill New York, 1994.

- [4] J. Fang, H. Li, Y. Tang, and F. Blaabjerg, "On the inertia of future more-electronics power systems," *IEEE Journal of Emerging and Selected Topics in Power Electronics*, 2018.
- [5] J. Liu, Y. Miura, and T. Ise, "Comparison of dynamic characteristics between virtual synchronous generator and droop control in inverter-based distributed generators," *IEEE Transactions on Power Electronics*, vol. 31, no. 5, pp. 3600–3611, 2016.
- [6] Y. Chen, R. Hesse, D. Turschner, and H.-P. Beck, "Improving the grid power quality using virtual synchronous machines," in *2011 International Conference on Power Engineering, Energy and Electrical Drives*, pp. 1–6. IEEE, 2011.
- [7] J. Driesen and K. Visscher, "Virtual synchronous generators," in *2008 IEEE Power and Energy Society General Meeting-Conversion and Delivery of Electrical Energy in the 21st Century*, pp. 1–3. IEEE, 2008.
- [8] T. Shintai, Y. Miura, and T. Ise, "Oscillation damping of a distributed generator using a virtual synchronous generator," *IEEE transactions on power delivery*, vol. 29, no. 2, pp. 668–676, 2014.
- [9] L. Xiong, F. Zhuo, F. Wang, X. Liu, Y. Chen, M. Zhu, and H. Yi, "Static synchronous generator model: a new perspective to investigate dynamic characteristics and stability issues of grid-tied pwm inverter," *IEEE Transactions on Power Electronics*, vol. 31, no. 9, pp. 6264–6280, 2015.
- [10] Q.-C. Zhong and G. Weiss, "Synchronverters: Inverters that mimic synchronous generators," *IEEE Transactions on Industrial Electronics*, vol. 58, no. 4, pp. 1259–1267, 2011.
- [11] W. Zhang, D. Remon, I. Candela, A. Luna, and P. Rodriguez, "Grid-connected converters with virtual electromechanical characteristics: experimental verification," *CSEE Journal of Power and Energy Systems*, vol. 3, no. 3, pp. 286–295, 2017.
- [12] H. Wu, X. Ruan, D. Yang, X. Chen, W. Zhao, Z. Lv, and Q.-C. Zhong, "Small-signal modeling and parameters design for virtual synchronous generators," *IEEE Transactions on Industrial Electronics*, vol. 63, no. 7, pp. 4292–4303, 2016.
- [13] J. Chen and T. O'Donnell, "Parameter constraints for virtual synchronous generator considering stability," *IEEE Transactions on Power Systems*, 2019.
- [14] F. Wang, L. Zhang, X. Feng, and H. Guo, "An adaptive control strategy for virtual synchronous generator," *IEEE Transactions on Industry Applications*, vol. 54, no. 5, pp. 5124–5133, 2018.
- [15] H. Wang, M. Liserre, F. Blaabjerg, P. de Place Rimmen, J. B. Jacobsen, T. Kvisgaard, and J. Landkildehus, "Transitioning to physics-of-failure as a reliability driver in power electronics," *IEEE Journal of Emerging and Selected Topics in Power Electronics*, vol. 2, no. 1, pp. 97–114, 2014.
- [16] D. Zhou, G. Zhang, and F. Blaabjerg, "Optimal selection of power converter in dfig wind turbine with enhanced system-level reliability," *IEEE Transactions on Industry Applications*, vol. 54, no. 4, pp. 3637–3644, 2018.
- [17] A. Sangwongwanich, Y. Yang, D. Sera, and F. Blaabjerg, "Mission profile-oriented control for reliability and lifetime of photovoltaic inverters," *IEEE Transactions on Industry Applications*, vol. 56, no. 1, pp. 601–610, 2020.
- [18] D. Zhou, H. Wang, and F. Blaabjerg, "Mission profile based system-level reliability analysis of dc/dc converters for a backup power application," *IEEE Transactions on Power Electronics*, vol. 33, no. 9, pp. 8030–8039, 2018.
- [19] M. G. Pecht, D. Das, and A. Ramakrishnan, "The iec standards on reliability program and reliability prediction methods for electronic equipment," *Microelectronics Reliability*, vol. 42, no. 9–11, pp. 1259–1266, 2002.
- [20] J. W. Harms, "Revision of mil-hdbk-217, reliability prediction of electronic equipment," in *2010 Proceedings-Annual Reliability and Maintainability Symposium (RAMS)*. IEEE, 2010, pp. 1–3.
- [21] G. Zeng, C. Herold, T. Methfessel, M. Schfer, O. Schilling, and J. Lutz, "Experimental investigation of linear cumulative damage theory with power cycling test," *IEEE Transactions on Power Electronics*, vol. 34, no. 5, pp. 4722–4728, 2019.
- [22] U. Choi, K. Ma, and F. Blaabjerg, "Validation of lifetime prediction of igt modules based on linear damage accumulation by means of superimposed power cycling tests," *IEEE Transactions on Industrial Electronics*, vol. 65, no. 4, pp. 3520–3529, 2018.
- [23] A. Hanif, Y. Yu, D. DeVoto, and F. Khan, "A comprehensive review toward the state-of-the-art in failure and lifetime predictions of power electronic devices," *IEEE Transactions on Power Electronics*, vol. 34, no. 5, pp. 4729–4746, 2019.



[24] J. V. M. Farias, A. F. Cupertino, V. d. N. Ferreira, H. A. Pereira, S. I. Seleme, and R. Teodorescu, "Reliability-oriented design of modular multilevel converters for medium-voltage statcom," *IEEE Transactions on Industrial Electronics*, vol. 67, no. 8, pp. 6206–6214, 2020.

[25] V. Raveendran, M. Andresen, G. Buticchi, and M. Liserre, "Thermal stress based power routing of smart transformer with chb and dab converters," *IEEE Transactions on Power Electronics*, vol. 35, no. 4, pp. 4205–4215, 2020.

[26] N. Sintamarean, F. Blaabjerg, H. Wang, F. Iannuzzo, and P. de Place Rimmen, "Reliability oriented design tool for the new generation of grid connected pv-inverters," *IEEE Transactions on Power Electronics*, vol. 30, no. 5, pp. 2635–2644, 2015.

[27] R. Fierro and F. Lewis, "Multilayer feedforward networks are universal approximators," *IEEE Trans. Syst., Man, Cybern.*, vol. 29, no. 6, pp. 649–654, 1999.

[28] Y. LeCun, Y. Bengio, and G. Hinton, "Deep learning," *nature*, vol. 521, no. 7553, pp. 436–444, 2015.

[29] T. Dragicevic, P. Wheeler, and F. Blaabjerg, "Artificial intelligence aided automated design for reliability of power electronic systems," *IEEE Transactions on Power Electronics*, 2018.

[30] J. He and Y. W. Li, "Analysis, design, and implementation of virtual impedance for power electronics interfaced distributed generation," *IEEE Transactions on Industry Applications*, vol. 47, no. 6, pp. 2525–2538, 2011.

[31] X. Meng, J. Liu, and Z. Liu, "A generalized droop control for grid-supporting inverter based on comparison between traditional droop control and virtual synchronous generator control," *IEEE Transactions on Power Electronics*, 2018.

[32] J. Fang, H. Li, Y. Tang, and F. Blaabjerg, "Distributed power system virtual inertia implemented by grid-connected power converters," *IEEE Transactions on Power Electronics*, vol. 33, no. 10, pp. 8488–8499, 2018.

[33] J. M. Hogg, Robert V. and A. T. Craig, *Introduction to mathematical statistics*. Pearson Education, 2005.

[34] "National grid. frequency data for 2018." [Online]. Available: <https://www.nationalgrideso.com/balancing-services/frequencyresponse-services/historic-frequency-data>.

[35] K. Chang, "Multiobjective optimization and advanced topics," *Design Theory and Methods Using CAD/CAE*, pp. 325–406, 2015.

[36] Y. P. K. G. Panchal, A. Ganatra and D. Panchal, "Behaviour analysis of multilayer perceptrons with multiple hidden neurons and hidden layers," *Int. J. Comput. Theory Eng.*, vol. 3, no. 2, p. 332, 2011.

[37] D. E. Rumelhart, G. E. Hinton, and R. J. Williams, "Learning internal representations by error propagation," California Univ San Diego La Jolla Inst for Cognitive Science, Tech. Rep., 1985.

[38] "Matlab Deep Learning Toolbox." [Online]. Available: <https://www.mathworks.com/products/deep-learning.html>.

[39] R. S. Figliola and D. E. Beasley, "Theory and design for mechanical measurements," John Wiley and Sons, NY, Fourth Edition, 2006.



**Tomislav Dragievi** (S09-M13-SM17) received the M.Sc. and the industrial Ph.D. degrees in Electrical Engineering from the Faculty of Electrical Engineering, Zagreb, Croatia, in 2009 and 2013, respectively. From 2013 until 2016 he has been a Postdoctoral research associate at Aalborg University, Denmark. From March 2016 until March 2020 he was an Associate Professor at Aalborg University, Denmark. From April 2020 he is a Professor at the Technical University of Denmark. He made a guest professor stay at Nottingham University, UK during spring/summer of 2018. His research interest is application of advanced control, optimization and artificial intelligence inspired techniques to provide innovative and effective solutions to emerging challenges in design, control and cyber-security of power electronics intensive electrical distributions systems and microgrids. He has authored and co-authored more than 220 technical publications (more than 100 of them are published in international journals, mostly in IEEE), 8 book chapters and a book in the field. He serves as an Associate Editor in the IEEE TRANSACTIONS ON INDUSTRIAL ELECTRONICS, in IEEE TRANSACTIONS ON POWER ELECTRONICS, in IEEE Emerging and Selected Topics in Power Electronics and in IEEE Industrial Electronics Magazine. Dr. Dragievi is a recipient of the Konar prize for the best industrial PhD thesis in Croatia, a Robert Mayer Energy Conservation award, and he is a winner of an Alexander von Humboldt fellowship for experienced researchers. He is currently listed as one of the top 5 trending authors in Engineering globally by Microsoft Academic



**Qianwen Xu** (S'14-M'18) received the B.Sc. degree from Tianjin University, China in 2014 and PhD degree from Nanyang Technological University, Singapore in 2018, both in electrical engineering. Then she worked as a research associate in Hong Kong Polytechnic University, a postdoc research fellow in Aalborg University in Denmark, a Wallenberg-NTU Presidential Postdoc Fellow in Nanyang Technological University in Singapore. She was also a visiting researcher with Imperial College London during March 2020 to June 2020. Currently she is

an assistant professor in Department of Electric Power and Energy Systems, KTH Royal Institute of Technology, Sweden. She was also awarded Alexander von Humboldt Fellowship, Chinese Government Award for Outstanding Students Abroad, Excellent Doctorate Research Work in Nanyang Technological University, Best paper award in IEEE PEDG 2020, etc. Her research interests include advanced control, optimization, stability and cybersecurity of microgrids and power electronics based power systems.



**Lihua Xie** received the Ph.D. degree in electrical engineering from the University of Newcastle, Australia, in 1992. Since 1992, he has been with the School of Electrical and Electronic Engineering, Nanyang Technological University, Singapore, where he is currently a professor and Director, Delta-NTU Corporate Laboratory for Cyber-Physical Systems. He served as the Head of Division of Control and Instrumentation from July 2011 to June 2014. He held teaching appointments in the Department of Automatic Control, Nanjing University of Science and Technology from 1986 to 1989.

Dr Xies research interests include robust control and estimation, networked control systems, multi-agent networks, localization and unmanned systems. He is an Editor-in-Chief for Unmanned Systems and an Associate Editor for IEEE Transactions on Network Control Systems. He has served as an editor of IET Book Series in Control and an Associate Editor of a number of journals including IEEE Transactions on Automatic Control, Automatica, IEEE Transactions on Control Systems Technology, and IEEE Transactions on Circuits and Systems-II. He was an IEEE Distinguished Lecturer (Jan 2012 Dec 2014) and an elected member of Board of Governors, IEEE Control System Society (Jan 2016-Dec 2018). Dr Xie is Fellow of IEEE, Fellow of IFAC and Fellow of Chinese Automation Association.



**Frede Blaabjerg** (S86M88SM97F03) was with ABB-Scandia, Randers, Denmark, from 1987 to 1988. From 1988 to 1992, he got the PhD degree in Electrical Engineering at Aalborg University in 1995. He became an Assistant Professor in 1992, an Associate Professor in 1996, and a Full Professor of power electronics and drives in 1998. From 2017 he became a Villum Investigator. He is honoris causa at University Politehnica Timisoara (UPT), Romania and Tallinn Technical University (TTU) in Estonia.

His current research interests include power electronics and its applications such as in wind turbines, PV systems, reliability, harmonics and adjustable speed drives. He has published more than 600 journal papers in the fields of power electronics and its applications. He is the co-author of four monographs and editor of ten books in power electronics and its applications.

He has received 31 IEEE Prize Paper Awards, the IEEE PELS Distinguished Service Award in 2009, the EPE-PEMC Council Award in 2010, the IEEE William E. Newell Power Electronics Award 2014, the Villum Kann Rasmussen Research Award 2014 and the Global Energy Prize in 2019. He was the Editor-in-Chief of the IEEE TRANSACTIONS ON POWER ELECTRONICS from 2006 to 2012. He has been Distinguished Lecturer for the IEEE Power Electronics Society from 2005 to 2007 and for the IEEE Industry Applications Society from 2010 to 2011 as well as 2017 to 2018. In 2019-2020 he serves a President of IEEE Power Electronics Society. He is Vice-President of the Danish Academy of Technical Sciences too. He is nominated in 2014-2018 by Thomson Reuters to be between the most 250 cited researchers in Engineering in the world.